# A Push-Pull Mechanism Helps Design Highly Competent G-Quadruplex-DNA Catalysts

Jielin Chen, Jiawei Wang, Stephanie van Der Lubbe, Mingpan Cheng, Dehui Qiu, David Monchaud, Jean-louis Mergny, Célia Fonseca Guerra, Huangxian Ju, Jun Zhou

CCS Chemistry

RESEARCH ARTICLE

Received: Aug. 14, 2020 | Accepted: Sept. 30, 2020

# A Push–Pull Mechanism Helps Design Highly Competent G-Quadruplex-DNA Catalysts

Jielin Chen[1†], Jiawei Wang[1†], Stephanie C. C. van der Lubbe[2†], Mingpan Cheng[1†], Dehui Qiu[1], David Monchaud[3], Jean-Louis Mergny[1], Célia Fonseca Guerra[2,4]*, Huangxian Ju[1]* & Jun Zhou[1]*

[1]*State Key Laboratory of Analytical Chemistry for Life Science, School of Chemistry and Chemical Engineering, Nanjing University, Nanjing 210023,* [2]*Theoretical Chemistry, Department of Chemistry and Pharmaceutical Sciences, AIMMS, Vrije Universiteit Amsterdam, Amsterdam 1081 HV,* [3]*Institut de Chimie Moléculaire (ICMUB), CNRS, Université de Bourgogne Franche-Comté, Dijon 21078,* [4]*Leiden Institute of Chemistry, Gorlaeus Laboratories, Leiden University, Leiden 2333 CD*

**Corresponding authors: c.fonsecaguerra@vu.nl; hxju@nju.edu.cn; jun.zhou@nju.edu.cn;* [†] J. Chen, J. Wang, S.C.C. van der Lubbe, and M. Cheng contributed equally to this work.

**Cite this:** *CCS Chem*. **2020**, *2*, 2183–2193

**Massive efforts are currently being invested to improve the performance, versatility, and scope of applications of nucleic acid catalysts. G-quadruplex (G4)/hemin DNAzymes are of particular interest owing to their structural programmability and chemical robustness. However, optimized catalytic efficiency is still bottleneck and the activation mechanism is unclear. Herein, we have designed a series of parallel G4s with different proximal cytosine (dC) derivatives to fine-tune the hemin-binding pocket for G4-DNAzymes. Combining theoretical and experimental methods, we have assessed the dependence of catalytic enhancement on the electronic properties of proximal dCs and demonstrated how proximal dCs activate catalytic proficiency. These results provide interesting clues in recapitulating the push–pull mechanism as the basis of peroxidase activity and help to devise a new strategy to design highly competent DNA catalysts whose performances are of the same order as protease.**

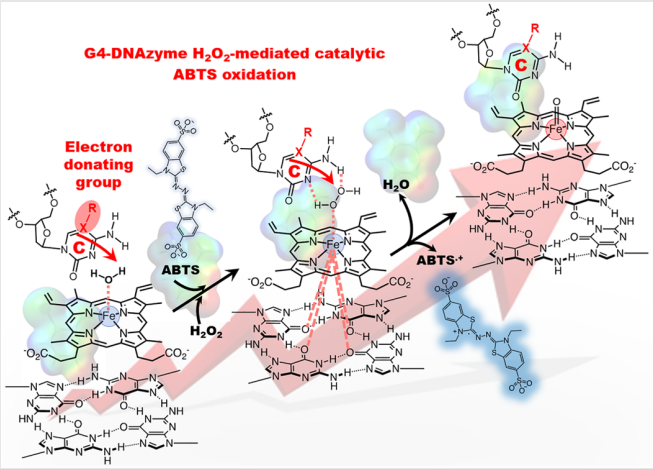


*Keywords:* **DNAzyme, electron density, G-quadruplex, hemin, push–pull mechanism**

## Introduction

The catalytic capability of nucleic acids was first reported with the study of self-splicing RNAs, or ribozymes, by Kruger et al.[1] and Guerriertakada,[2] and of RNA-cleaving DNA enzymes, or DNAzymes, by Breaker and Joyce.[3] Afterward, both ribozymes and DNAzymes were implemented as efficient biodevices in different fields including biosensing, chemical transformations, and chemical biology.[4–7] G-quadruplex (G4)-DNAzymes represent a particular class of DNAzymes in which a four-stranded G4-DNA interacts with the cofactor hemin to perform hemoenzyme-type reactions.[8–12] The current popularity of G4-DNAzymes stems from the versatile

DOI: 10.31635/ccschem.020.202000473
*CCS Chem.* **2020**, *2*, 2183–2193

designability[13-17] and excellent biocompatibility of G4 precatalysts.[18-21] Unfortunately, the performances of G4-DNAzymes are still below those of corresponding enzymes, leading to new research and strategies for improved performance. To date, optimization strategies can be divided into two types: the addition of exogenous activators,[22-29] such as spermine,[22] cytidine triphosphate (CTP),[23] adenine triphosphate (ATP),[23-25] template-assembled synthetic G-quartet (TASQ),[26] and self-assembling peptides[27-29] on one side, and the modification of the G4 structure[30-35] to provide hemin with a more defined and suited binding pocket[31,32] or hemin itself[36,37] on the other side. The latter mostly focuses on the modification of the so-called parallel G4 structure, in which all constitutive DNA strands are codirectionally oriented and the structure displays fairly accessible G-quartets, the privileged hemin-binding site.[38] Efforts have been invested to fine-tune G4 structures to improve their catalytic performances, notably modifying the sequences flanking the external G-quartet,[31,34,35,39] as well as the loops and bulges of the G4 core.[33] As an example, it was demonstrated that polyadenine and polycytosine tails positively impact catalytic performance.[31,33,35]

Efforts have also been invested to better understand the mechanisms behind these catalytic improvements. Travascio et al. implemented UV–vis[9] and electron paramagnetic resonance (EPR)[10] spectroscopies to provide a convincing model for a G4/hemin system. Yamamoto et al.[36,40] scrutinized the coordination of the hemin iron atom to gain reliable insights into the hemin/G-quartet interactions by both vibrational and nuclear magnetic resonance (NMR) spectroscopies. We and others have exploited the Lewis acid-base theory to demonstrate the synergistic cooperation of hemin activation between the external G-quartet and its proximal nucleotides.[31,34]

Herein, we take a further leap toward the elucidation of the actual G4-DNAzyme mechanism, demonstrating how the axial coordination of proximal dC activates hemin in a peroxidase-mimicking manner. Our approach was nature-driven: in the catalytic cycle of the model horseradish peroxidase (HRP), the so-called push–pull mechanism is central.[41-44] As shown in Supporting Information Figure S1, the push effect being provided by the histidine 170 (His170) stabilizes the higher oxidation states of the iron atom during catalysis, and the pull effect being mediated by the His42 acting together with the Arg38 facilitates heterolytic O–O bond cleavage of the iron-bound hydrogen peroxide (the stoichiometric oxidant). Thus, we decided to modulate the electron density of the proximal dC to investigate whether and to which extent it influences the G4-DNAzyme activity. Our results demonstrate that electron-rich dCs strengthen the hydrogen bond with $H_2O_2$ and boost the Compound $0 \rightarrow 0^* \rightarrow 1$ transfer in a His42-like manner, which leads to notable catalytic enhancements.[23,45]

# Experimental Methods

## Materials and reagents

Oligonucleotides, purified by HPLC, were purchased from Sangon Biotech (Shanghai, China) and Takara Biomedical Technology (Dalian, China), dissolved in ultrapure water (18.2 MΩ·cm) and used without further treatment. The concentrations of oligonucleotides were determined by the UV–vis absorbance at 260 nm, using the molar extinction coefficients provided by OligoAnalyzer 3.1 (http://sg.idtdna.com/calc/analyzer). About 100 mM Britton–Robinson buffer (B–R buffer) was prepared with 0.5 M $H_3BO_3$, 0.5 M $H_3PO_4$, and 0.5 M $CH_3COOH$ and titrated with 1 M KOH to pH 7.0. All experiments were performed in 10 mM B–R buffer (pH 7.0 except pH-dependence experiments) containing 0.05% Triton X-100, 0.1% DMSO, and 100 mM KCl. G4s (10 μM) were prepared in 10 mM B–R buffer, with 100 mM $K^+$, heated to 95 °C for 5 min, cooled slowly to room temperature, and stored at 4 °C overnight prior to use. Hemin stock solution was prepared with DMSO. About 50 mM 2,2′-azino-bis-(3-ethylbenzothiozoline-6-sulfonic acid) (ABTS), β-nicotinamide adenine dinucleotide (NADH), and $H_2O_2$ were freshly prepared every time in ultrapure water and 50 mM 3,3′,5,5′-tetramethylbenzidine (TMB) in DMSO. All chemicals were obtained from Sigma (St. Louis, USA).

## Circular dichroism measurements

About 5 μM G4 solutions were obtained by directly diluting stock solutions with 10 mM B–R buffer. Circular dichroism (CD) spectra were collected with three measurements on a Chirascan CD spectrometer (Applied Photophysics, Leatherhead, UK) in the wavelength range of 220–335 nm at 25 °C.

## Activity measurements of G4-DNAzymes

About 0.4 μM G4s were incubated at 25 °C with 0.8 μM hemin in the B–R buffer (pH 7.0) for 2 h. After the formation of G4/hemin complexes, ABTS (0.6 mM, final concentration) was first added, and then variable concentrations of $H_2O_2$ were added, with final concentrations of 0.1, 0.15, 0.2, 0.3, 0.5, 1, 2.5, 5, and 10 mM to start the reactions, where the absorbance of $ABTS^{\cdot+}$ at 414 nm was monitored for 60 s by a Cary100 (Agilent, Santa Clara, USA) spectrophotometer. To further confirm DNAzyme activity, the other two substrates, TMB and NADH, were chosen. The absorbance of $TMB^{\cdot+}$ at 652 nm and NADH at 340 nm was recorded for 60 s. The extinction coefficient for $ABTS^{\cdot+}$ at 414 nm was 36,000 $M^{-1}$ $cm^{-1}$; $TMB^{\cdot+}$ at 652 nm was 39,000 $M^{-1}$ $cm^{-1}$; and NADH at 340 nm was 6220 $M^{-1}$ $cm^{-1}$.[9,34]

The initial rate ($V_0$, nM $s^{-1}$) of the oxidation reaction was calculated with the slope of the plot of absorbance versus reaction time in initial 10 s. The Michaelis constant,

DOI: 10.31635/ccschem.020.202000473
*CCS Chem.* **2020**, *2*, 2183–2193

$K_m$, was obtained with the Michaelis–Menten model. All kinetic measurements were repeated three times, and the background activity of hemin alone was subtracted.

To examine the dependence of G4-DNAzyme activity on pH, the G4-DNAzyme activity was measured in 10 mM B–R buffers at different pHs from 3.0 to 8.0. After G4s (0.4 μM) were incubated with 0.8 μM hemin at 25 °C for 2 h, 0.6 mM ABTS and 0.6 mM $H_2O_2$ were added to initiate the reaction.

## Computational settings

All calculations were performed with the density functional theory (DFT)-based program Amsterdam Density Functional (ADF) 2017.208 at the ZORA-BLYP-D3(BJ)/TZ2P level of theory for geometric optimization and binding energies.[46–51] Geometries were optimized in implicit chloroform solvation with $C_1$ (i.e., without) symmetry constraints because the dielectric constant ε of chloroform (ε = 4.8) is close to the experimentally determined dielectric constant of DNA (ε ≈ 8).[52] All optimized structures have been verified to be true minima through vibrational analysis (zero imaginary frequencies). The binding energies Δ$E$ were obtained by eq 1:

$$\Delta E = E_{\text{dimer}} - E_{\text{monomer1}} - E_{\text{monomer2}} \quad (1)$$

where $E_{\text{dimer}}$ and $E_{\text{monomer}}$ are the energies of the optimized dimers and monomers, respectively. Full computational details are given in the Supporting Information.

## Voronoi deformation density charges

The atomic charge distribution was analyzed using the Voronoi deformation density (VDD) method.[53] The VDD method partitions the space into so-called Voronoi cells, which are nonoverlapping regions of space that are closer to nucleus A than to any other nucleus. The charge distribution was determined by taking a fictitious promolecule as a reference point, in which the electron density was simply the superposition of the atomic densities. The change in density in the Voronoi cell when going from this promolecule to the final molecular density of the interacting system is associated with the VDD atomic charge ($Q^{\text{VDD}}$). Thus, the VDD atomic charge of atom A is given by eq 2:

$$Q_{\text{A}}^{\text{VDD}} = -\int_{\text{voronoi cell of A}} [\rho(\boldsymbol{r}) - \rho_{\text{promolecule}}(\boldsymbol{r})]\,d\boldsymbol{r} \quad (2)$$

Therefore, instead of computing the amount of charge contained in an atomic volume, we computed the flow of charge from one atom to the other upon molecular formation. Therefore, the physical interpretation was straightforward. A positive atomic charge $Q_{\text{A}}^{\text{VDD}}$ corresponds to a loss of electrons, whereas a negative atomic charge $Q_{\text{A}}^{\text{VDD}}$ is associated with a gain of electrons in the Voronoi cell of atom A. This effectively means that the more electron-rich N3 atoms have a lower (i.e., more negative) VDD charge.

# Results and Discussion

## Proximal dC derivative designation for G4-DNAzymes

It is now established that while hemin may bind to the two external G-quartets of a G4, it acquires better

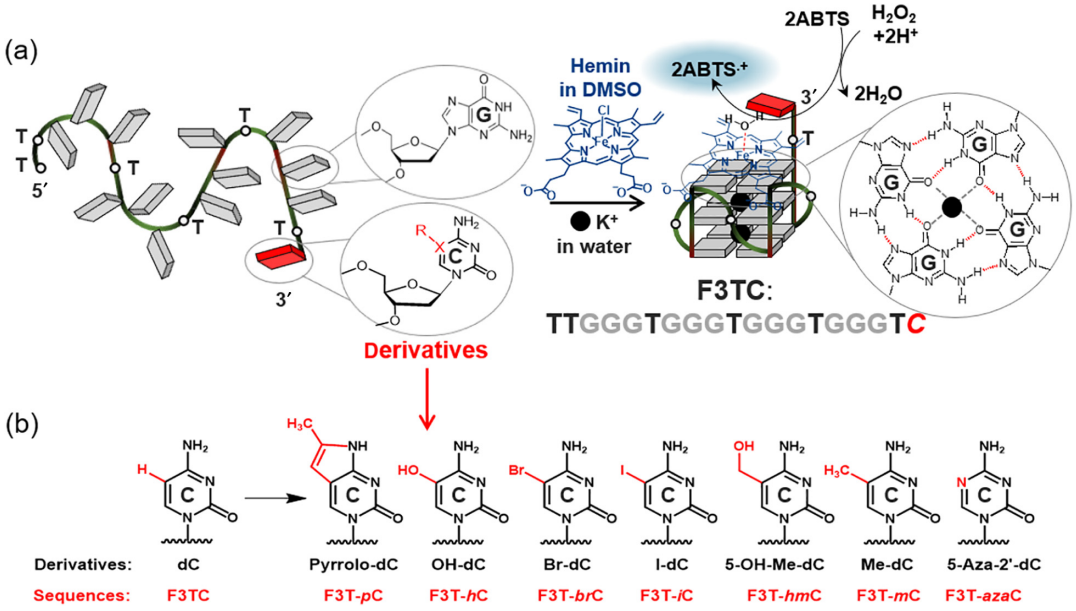


**Figure 1** | *Schematic illustration of the G4-DNAzyme. (a) F3TC used as a model sequence. (b) Different dC derivatives used in this study.*

DOI: 10.31635/ccschem.020.202000473
*CCS Chem.* **2020**, *2*, 2183–2193

catalytic performances atop the 3′-terminal G-quartet.[31,34] We also demonstrated that a proximal dC located near the 3′-terminal efficiently enhances the catalytic activity of the corresponding G4.[34] Therefore, we decided to further optimize the structure of F3TC (d[$T_2G_3TG_3TG_3TG_3TC$]), a parallel G4 tailed with a 3′-terminal dC that can be substituted by a variety of modified nucleobases (Figure 1a).

The dC was modified to modulate its electron density to assess the consequence of this modification on G4 catalytic efficiency, performing the oxidation of the dye ABTS as a model reaction in light of its readily monitorable output (Figure 2a). The electron density of dC was modulated by introducing different chemical groups on the dC core, changing the H5 hydrogen atom for OH (OH-dC, F3T-*h*C), bromine (Br-dC, F3T-*br*C), iodine (I-dC, F3T-*i*C), $CH_2OH$ (5-OH-Me-dC, F3T-*hm*C), or $CH_3$ (Me-dC, F3T-*m*C), C5 for N5 (5-Aza-2′-dC, F3T-*aza*C), or merging an additional pyrrole ring (Pyrrolo-dC, F3T-*p*C) (Figure 1b and Supporting Information Table S1). Circular dichroism spectra (Supporting Information Figure S2) confirmed that all these sequences adopt parallel G4 conformation, indicating that dC derivatives did not affect the G4 formation and its overall topology.

The electronic consequences of these derivatives were studied by analyzing the electrostatic potential surfaces (EPSs) (Figure 2b). The EPSs of the dC derivatives are close to the wild-type dC, with a negative charge accumulation centered on the N3 atom.[46–51] To further quantify any differences between the various derivatives, we analyzed the atomic charges by using the VDD method.[53] All N3 atoms in all dC derivatives possess a negative charge (Figure 2c), which is in line with the EPSs. The negative VDD charge ($Q^{VDD}$) accumulation is most pronounced in dC [$Q^{VDD} = -305$ milli-electrons ($me^-$)], and the least amount of accumulation occurs in Br-dC and I-dC (−289 $me^-$). The VDD charges of Me-dC (−303 $me^-$) and 5-Aza-2′-dC (−303 $me^-$) are approximately the same as the wild-type dC (−305 $me^-$).

## Catalytic activity characterization

The $H_2O_2$-mediated oxidation of ABTS catalyzed by dC-modified G4-DNAzymes was monitored via the

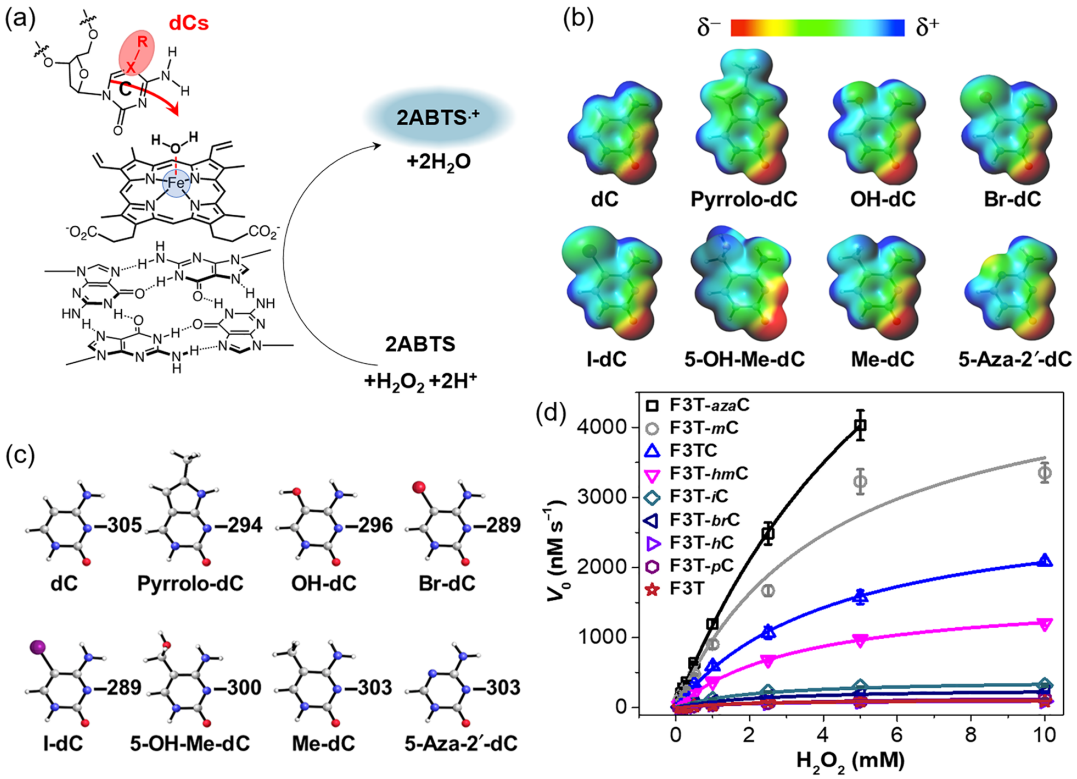


**Figure 2** | *(a) Peroxidation reaction facilitated by G4-DNAzyme for oxidation of ABTS by $H_2O_2$. (b) Electrostatic potential surface (at 0.005 a.u.) from −0.1 (red) to 0.1 (blue) a.u. for prepared cytosine derivatives computed at the ZORA-BLYP-D3(BJ)/TZ2P level of theory in implicit chloroform solvation. (c) $Q^{VDD}$ (in $me^-$) on N3 atom in different cytosine derivatives in implicit chloroform solvation, obtained at the ZORA-BLYP-D3(BJ)/TZ2P level of theory. (d) Saturation curves for ABTS oxidation catalyzed by different G4-DNAzymes in the presence of $H_2O_2$ with increasing concentration.*

DOI: 10.31635/ccschem.020.202000473
*CCS Chem.* **2020**, *2*, 2183–2193

**Table 1** | *Kinetic Parameters of Various Derivatives DNAzyme with Respect to the Catalysis of ABTS to ABTS·+*[a]

| Sequences[b] | $K_m$ (mM) | $V_{max}$ (μM $s^{-1}$) | $k_{cat}$ ($s^{-1}$) | $k_{cat}/K_m$ ($s^{-1}$·$mM^{-1}$) | $k_{cat}/k_O$[c] |
|---|---|---|---|---|---|
| F3T | 1.80 ± 0.41 | 0.12 ± 0.01 | 0.30 ± 0.02 | 0.17 | 1.0 |
| F3T-*p*C | 3.70 ± 0.48 | 0.17 ± 0.01 | 0.42 ± 0.02 | 0.11 | 1.4 |
| F3T-*h*C | 1.87 ± 0.24 | 0.11 ± 0.01 | 0.28 ± 0.01 | 0.15 | 0.9 |
| F3T-*br*C | 2.26 ± 0.21 | 0.28 ± 0.01 | 0.69 ± 0.02 | 0.30 | 2.3 |
| F3T-*i*C | 2.17 ± 0.25 | 0.40 ± 0.02 | 1.01 ± 0.04 | 0.47 | 3.4 |
| F3T-*hm*C | 3.47 ± 0.13 | 1.64 ± 0.03 | 4.09 ± 0.07 | 1.18 | 13.6 |
| F3TC | 4.34 ± 0.20 | 2.97 ± 0.06 | 7.44 ± 0.15 | 1.72 | 24.8 |
| F3T-*m*C | 4.22 ± 1.17 | 5.07 ± 0.63 | 12.68 ± 1.58 | 3.00 | 42.3 |
| F3T-*aza*C | 7.62 ± 0.28 | 10.15 ± 0.25 | 25.39 ± 0.63 | 3.33 | 84.6 |

[a] Conditions: 0.1–10 mM $H_2O_2$, 0.6 mM ABTS, 0.4 μM G4/hemin DNAzyme.
[b] Sequences are shown in Supporting Information Table S1.
[c] $k_O = (0.30 \pm 0.02)$ $s^{-1}$, $k_{cat} = V_{max}/0.4$ μM.

time-dependent absorbance change at 414 nm, characteristic of the ABTS·+ formation[9] (Figure 2d and Supporting Information Figure S3). All dC-modified G4-DNAzymes were found to be more catalytically proficient than F3T (d[$T_2G_3TG_3TG_3TG_3T$]), but F3T-*aza*C (C5 to N5 substitution) and F3T-*m*C were found to be more efficient than F3TC. F3T-*aza*C exhibited the $k_{cat}$ and $K_m$ values of 25.39 ± 0.63 $s^{-1}$ and 7.62 ± 0.28 mM, respectively, versus 12.68 ± 1.58 $s^{-1}$ and 4.22 ± 1.17 mM for F3T-*m*C (Table 1), obtained according to Michaelis–Menten model (Supporting Information Figure S4). The $k_{cat}$ and $K_m$ values of F3T-*aza*C and F3T-*m*C were 3.4- and 1.7-fold ($k_{cat}$), and 1.8- and 0.97-fold ($K_m$) those of F3TC, 84.6- and 42.3-fold ($k_{cat}$), and 4.2- and 2.3-fold ($K_m$) those of F3T. The $k_{cat}$ value of F3T-*aza*C was close to native enzymes HRP, which varies between 50 and 800 $s^{-1}$ depending on the circumstances.[54,55] Of note, under the same reaction conditions of F3T-*aza*C, the measured $k_{cat}$ value of HRP was 578 $s^{-1}$ (Supporting Information Figure S5). Interestingly, the catalytic activity of these different dC derivatives-based G4-DNAzyme was further confirmed through the oxidation of the other two substrates, TMB and NADH, and showed the same trend with ABTS (Supporting Information Figure S6).

## Potential mechanism for the dependence of G4-DNAzyme activity on proximal dC electron density

To gain insights into how the electron density of dC influences catalysis, we next focused on the first catalytic stage of G4-DNAzyme, that is, the conversion of Compound 0 [coordination of $H_2O_2$ to the hemin Fe(III) atom] to Compound 0* (heterolytic cleavage of $H_2O_2$) to ultimately produce Compound 1 (vide infra). We monitored these steps via UV–vis measurements in the absence of ABTS substrate (Supporting Information Figures S7 and S8) to quantify the $H_2O_2$-mediated oxidative degradation of G4/hemin complexes. G4-DNAzymes showed characteristic peaks at 404, 504, and 630 nm (Soret bands), which decreased rapidly after the addition of $H_2O_2$, implying the oxidative decay of the Fe(III) intermediate, concomitantly with the band increase in the 550–620 and 650–700 nm regions, characteristic of Compound 1 formation (Supporting Information Figure S8).[10,31] The plot of initial degradation velocity

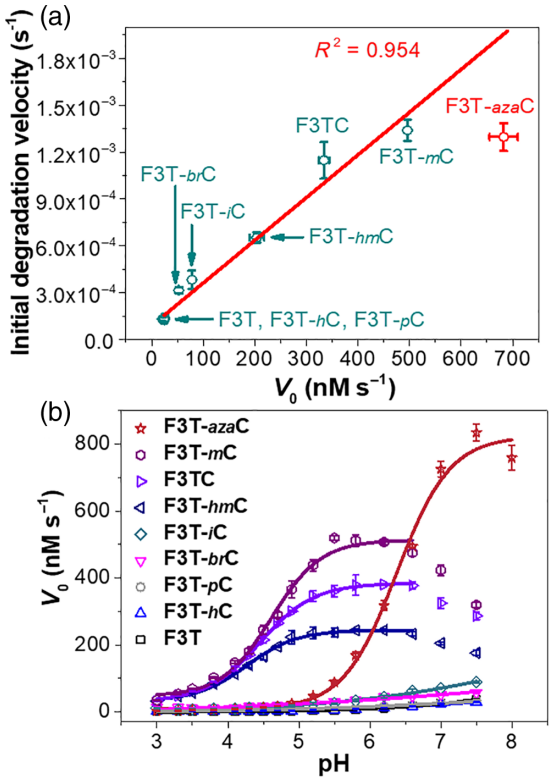


**Figure 3** | *(a) Correlation between initial degradation velocity and the activity ($V_O$) of G4-DNAzymes at 0.4 mM $H_2O_2$. Note: The initial degradation velocity for F3T-*azaC *was too fast to record, leading to a deviation of its observed velocity from the actual one. (b) Catalytic activity of G4-DNAzymes at different pHs.*

DOI: 10.31635/ccschem.020.202000473
*CCS Chem.* **2020**, *2*, 2183–2193

versus catalytic activity showed linear correlation (Figure 3a), in agreement with the involvement of dC electronic density in the formation of catalytic intermediates. A notable exception was F3T-*aza*C for which the decay rate was too fast to be reliably quantified.

Next, we focused on the formation of Compound 1, which is produced from Compound 0* after the loss of two electrons, one from the iron atom [which becomes Fe(IV)], and the other from the porphyrin ring. The formation of the catalytically active Fe(IV) is the rate-determining step of the catalysis. In the catalytic cycle of HRP, this step is promoted by His42 with a p$K_a$ of 2.5 (His42.H$^+$/His42), suitable to assist $H_2O_2$ cleavage since the p$K_a$ of the hemin-bound $H_2O_2/HO_2^-$ is between 3.2 and 4.0. In G4-DNAzymes, His42 is replaced by dC with a p$K_a$ of 4.1 (CTP.H$^+$/CTP), which is also compatible with this transfer.[23] We then evaluated the activity of dC-modified DNAzymes at pHs from 3.0 to 8.0 (Supporting Information Figure S9). The catalytic proficiency of these G4-DNAzymes was found to be sensitive to pH, and F3TC, F3T-*m*C, F3T-*hm*C, and F3T-*aza*C showed relatively high activity with plateaus after 5.0 for F3TC, F3T-*m*C, and F3T-*hm*C, and 7.0 for F3T-*aza*C (Figure 3b). The apparent p$K_a$ was found to be 4.2 for F3T-*hm*C, 4.4 for F3TC, 4.5 for F3T-*m*C, and 6.4 for F3T-*aza*C, respectively. The dependence of p$K_a$ on dCs was in line with VDD charge (between −300 and −305 me$^-$, Figure 2c), confirming that higher electron density on dCs induce higher apparent p$K_a$, making N3 harder to be deprotonated. These results further confirm the involvement of dC in the rate-determining step of the catalysis, thus mimicking the role of His42 in HRP.

The interaction between dCs and $H_2O_2$ was further investigated using DFT computations at the ZORA-BLYP-D3(BJ)/TZ2P level of theory in implicit chloroform solvation.[46-51] The computed binding energy ($\Delta E$) between dCs and $H_2O_2$ ranged between −10.7 and −11.5 kcal·mol$^{-1}$ (Figure 4a). For most dCs, the binding

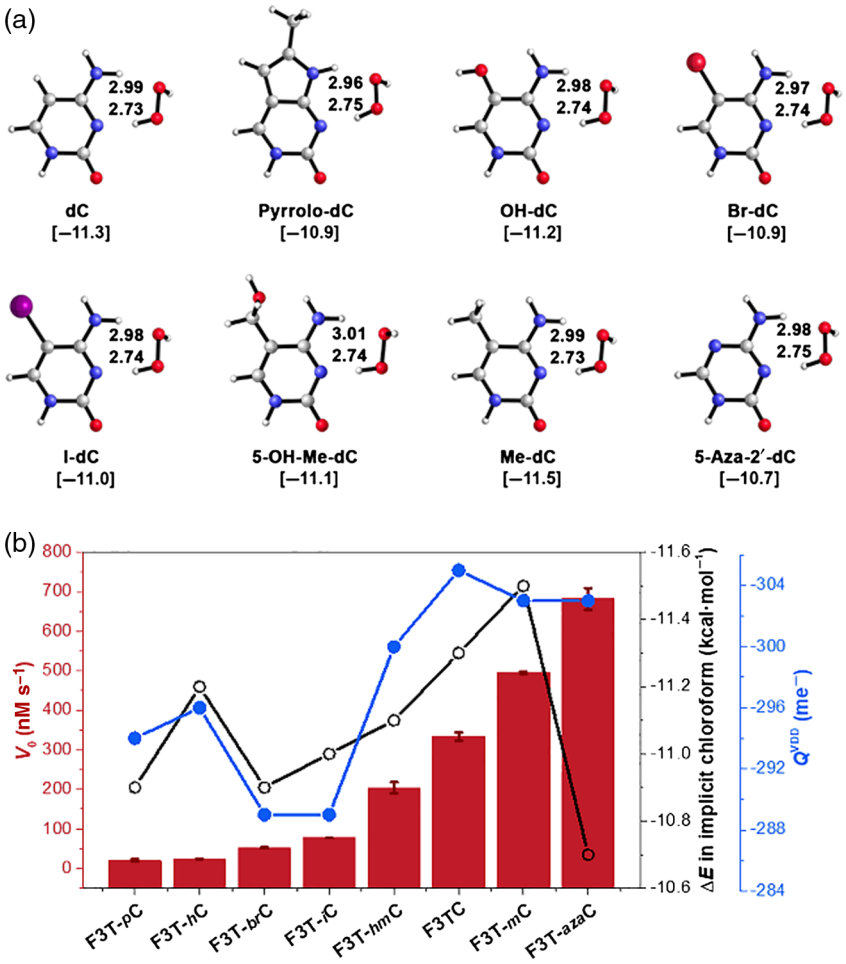


**Figure 4** | *(a) Optimized structures, binding energies* ΔE *(in kcal·mol$^{-1}$), and N–O distances (in Å) in implicit chloroform solvation, obtained at the ZORA-BLYP-D3(BJ)/TZ2P level of theory. (b) Activity (red columns) and computed binding energy (black line) of different DNAzymes with $H_2O_2$ at 0.6 mM, and $Q^{VDD}$ of different cytosine derivatives on N3 (blue line).*

DOI: 10.31635/ccschem.020.202000473
*CCS Chem.* **2020**, *2*, 2183–2193

energy ($\Delta E$) and N3 atomic charge ($Q^{VDD}$) showed positive correlation with experimental activity (Figure 4b), implying a simple electronically driven $H_2O_2$ coordination with dCs. However, disconnections were found for Pyrrolo-dC, OH-dC, and 5-Aza-2′-dC. For Pyrrolo-dC, the VDD charge (–294 me$^-$) and binding energy (–10.9 kcal·mol$^{-1}$) were relatively negative in comparison with its activity of 21.0 nM s$^{-1}$. This was probably caused by the absence of $NH_2$ group and the presence of NH incorporated in another ring, which affected the size of the Voronoi cell and the VDD charge. OH-dC displayed both more negative (i.e., more stable) binding energy (–11.2 kcal·mol$^{-1}$) and more negative VDD charge (–296 me$^-$) than anticipated, while 5-Aza-2′-dC displayed a N3 VDD charge of –303 me$^-$ but a more positive (i.e., less stable) binding energy than that suggested by the experimental activity (682.6 nM s$^{-1}$).

The observed discrepancies between $V_0$ values and the theoretical results for 5-Aza-2′-dC and OH-dC can be explained through their unique capability to form hydrogen (H) bonds with two binding faces. 5-Aza-2′-dC (with high $V_0$ but more positive $\Delta E$) can coordinate with $H_2O_2$ via both its N3 atom and its N5 atom (Figures 5a and Supporting Information Figure S10), while OH-dC (with low $V_0$ but more negative $\Delta E$) can coordinate with $H_2O_2$ via its additional OH group (Supporting Information Figure S11). Therefore, we computed $H_2O_2$ binding with 5-Aza-2′-dC and OH-dC on their secondary binding face. The $H_2O_2$-binding energy of 5-Aza-2′-dC N3-face (–10.7 kcal·mol$^{-1}$) is only 1.1-fold of its N5-face (–9.5 kcal·mol$^{-1}$, Supporting Information Figure S10c), while the $H_2O_2$-binding energy of OH-dC primary binding face (–11.2 kcal·mol$^{-1}$) is 2.1-fold of its secondary binding face (–5.4 kcal·mol$^{-1}$, Supporting Information Figure S11a). The near equivalence of the two 5-Aza-2′-dC faces explains why it is more catalytically proficient than the nonequivalent OH-dC. In addition, the OH group of OH-dC can be involved in an extended H-bond network with surrounding $H_2O$ molecules (Figure 5b and Supporting Information Figures S11b and S11c). We computed the influence of additional H bonds with three $H_2O$ molecules (two as H-bond acceptor, one as donor) on the N3 electron density. The additional H bonds resulted in the change of $Q^{VDD}$ on N3 atom from

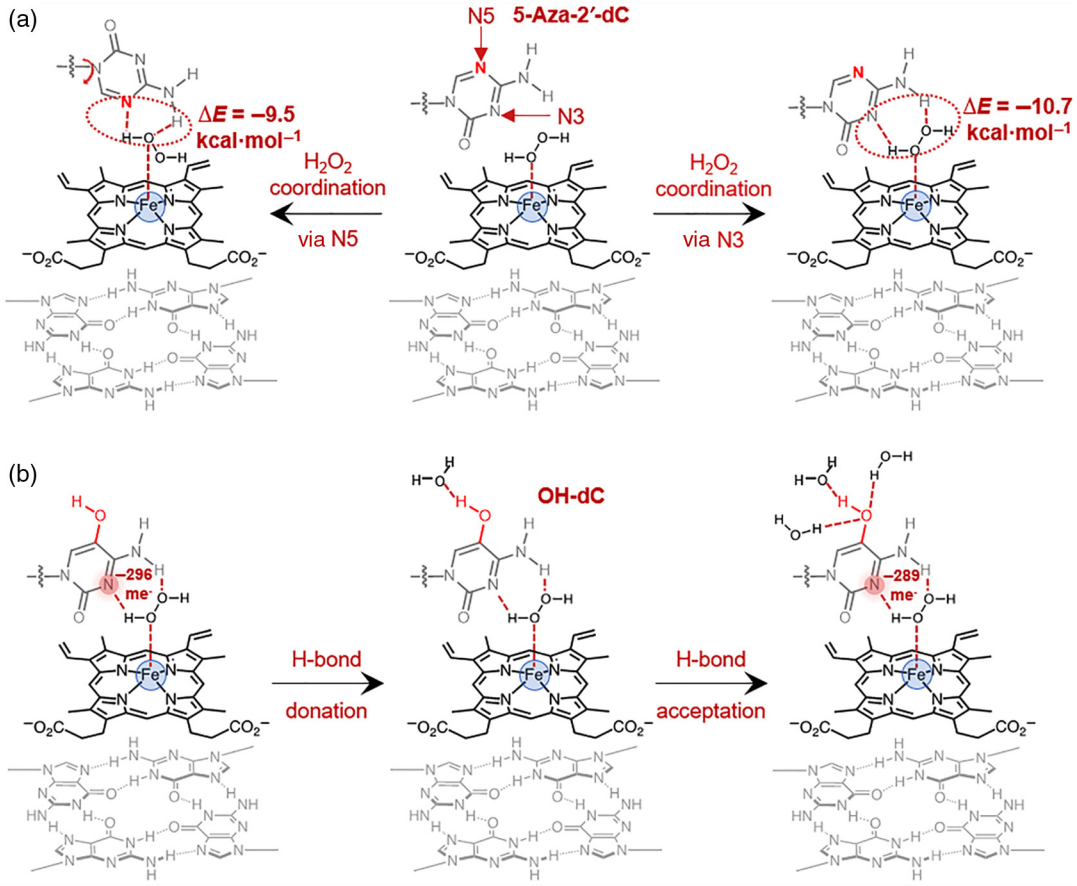


**Figure 5** | *Schematic representation of the double coordination for (a) 5-Aza-2′-dC in G4-DNAzyme with $H_2O_2$ and (b) the hydrogen bonds formed between OH-dC in G4-DNAzyme and $H_2O$. Details are shown in Supporting Information Figures S10 and S11. Blue spheres represent Fe(III).*

DOI: 10.31635/ccschem.020.202000473
*CCS Chem.* **2020**, *2*, 2183–2193

–296 to –289 me⁻ (Supporting Information Figures S11c and S11d), which provided a rationale for the lower catalytic proficiency of F3T-*h*C.

From a theoretical point of view, these results indicate that calculations for geometric optimization and binding energy must consider possible structural bias (e.g., nucleobase rotation) and environmental effects (e.g., hydration) to provide more accurate predictive models for DNAzyme catalytic cycles. From an experimental point of view, they cast a bright light on the performances of F3T-*aza*C, which brings DNA catalysts ever closer to hemoenzymes thanks to a quite unique, double, and synergistic $H_2O_2$-coordination site. Overall, we designed the experiments based on theoretical calculations, then obtained a highly active G4-based DNAzyme, and finally continued to verify the construction mechanism for our highly proficient enzymes through the push–pull mechanism.

The HRP mechanism has been thoroughly studied, and the central role of two histidine (His) residues, His42 and His170, in the hemin-binding site has been found to synergistically interact with hemin to perform catalytic peroxidation reactions (Supporting Information Figure S1).[41–44] These His, located on both sides of the hemin, activate the cofactor through a push–pull mechanism. The push effect is provided by proximal His170 via direct coordination to the hemin iron atom, and the pull effect is mediated by distal His42 via interaction with the oxidant $H_2O_2$. In G4-DNAzymes, the G-quartet on which the hemin stacks plays the role of His170, via a mechanism that is not yet fully understood,[30] while the role of His42 can be played by the proximal dCs (Figure 6). Here, we studied dCs as His42 surrogates, and the influence of their electron density on the catalytic activity of the resulting G4-DNAzyme systems. The electron density could be controlled via introduction of various dC derivatives as either electron-donating or electron-withdrawing groups. We demonstrated that the proximal dC with higher electron density led to higher catalytic activity of the G4-DNAzyme. The G4-DNAzymes (F3T-*m*C and F3T-*aza*C) containing two dC derivatives, Me-dC and 5-Aza-2′-dC, provided better catalytic performances than F3TC. Interestingly, these two G4s are representative examples exhibiting the intricate relationship between experiments and calculations: the former, F3T-*m*C, provided a linear correlation between predictions and results, with slightly more stable Δ*E* than F3TC that led to slightly better catalytic performances. This originated in the simple structure of Me-dC. The latter, F3T-*aza*C, highlighted that care must be taken in trying to recapitulate experimental conditions in silico, owing to

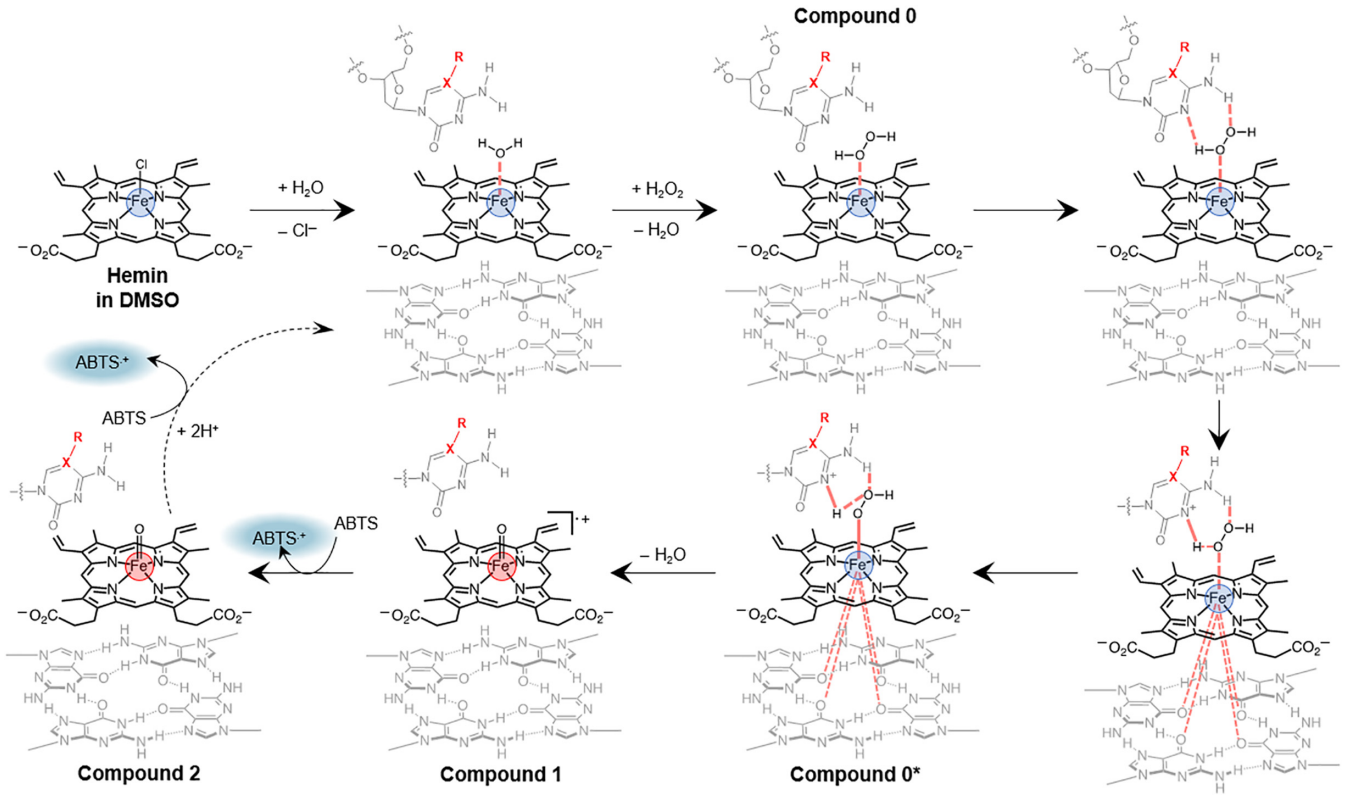


**Figure 6** | *Schematic representation of the catalytic cycle of G4-DNAzyme for the oxidation of ABTS to ABTS·⁺ by $H_2O_2$. Blue and red spheres represent Fe(III) and Fe(IV), respectively.*

DOI: 10.31635/ccschem.020.202000473
*CCS Chem.* **2020**, *2*, 2183–2193

possible structural and environmental bias. 5-Aza-2′-dC indeed provided multiple $H_2O_2$ anchoring points that bolstered its catalytic performances, for which a second round of computation could be readily accounted.

## Conclusion

Globally speaking, we found that dC electron density strongly impacted G4-DNAzyme catalysis, being directly involved in and fostering the formation of Compound 1. Thus, these results confirmed the key role of the push–pull mechanism on the electron-transfer process, in an HRP-like manner. We showed that a combination of experiment results and theoretical calculations provided insights into the fine mechanistic details of G4-DNAzyme inner workings. Each step of the catalytic cycle could be reliably computed, which opened broad perspectives as for the computer-aided design of ever more efficient DNAzyme systems. Here, we highlighted the intricate connection between electron density and $H_2O_2$-binding energy, which showed positive correlation with simple dC derivatives but more complicated with dC derivatives with an extended hydrogen-bond donating/accepting network. Therefore, to design a high-activity DNAzyme, future adjacent nucleotides may need to have the following characteristics: contain both hydrogen-bond donor and acceptor to form a hydrogen-bond network with $H_2O_2$; high electron density; and form multiple binding surfaces with $H_2O_2$ to promote the heterolysis of $H_2O_2$ and accelerate the formation of Compound 1. Thus, our approach provided a new way to design ever more effective DNA catalysts, which now achieve a level of performance in the same order as proteinaceous catalysts.

## Supporting Information

Supporting Information is available.

## Conflict of Interest

There is no conflict of interest to report.

## Acknowledgments

The authors acknowledge the financial support of the National Natural Science Foundation of China (nos. 21977045 and 21635005), the Fundamental Research Funds for the Central Universities (no. 02051430210), the Technology Innovation Fund Project of Nanjing University (no. 020514913415), the Excellent Research Program of Nanjing University (no. ZYJH004), the funds of Nanjing University (no. 020514912216), the Netherlands Organization for Scientific Research (NWO/CW), the CNRS, Agence Nationale de la Recherche (no. ANR-17-CE17-0010-01), Université de Bourgogne and Conseil Régional de Bourgogne (PARI), and the European Union (PO FEDER-FSE Bourgogne 2014/2020 programs).

## References

1. Kruger, K.; Grabowski, P. J.; Zaug, A. J.; Sands, J.; Gottschling, D. E.; Cech, T. R. Self-Splicing RNA: Autoexcision and Autocyclization of the Ribosomal RNA Intervening Sequence of Tetrahymena. *Cell* **1982**, *31*, 147–157.
2. Guerriertakada, C.; Gardiner, K.; Marsh, T.; Pace, N.; Altman, S. The RNA Moiety of Ribonuclease P Is the Catalytic Subunit of the Enzyme. *Cell* **1983**, *35*, 849–857.
3. Breaker, R. R.; Joyce, G. F. A DNA Enzyme that Cleaves RNA. *Chem. Biol.* **1994**, *1*, 223–229.
4. Willner, I.; Shlyahovsky, B.; Zayats, M.; Willner, B. DNAzymes for Sensing, Nanobiotechnology and Logic Gate Applications. *Chem. Soc. Rev.* **2008**, *37*, 1153–1165.
5. Liu, J.; Cao, Z.; Lu, Y. Functional Nucleic Acid Sensors. *Chem. Rev.* **2009**, *109*, 1948–1998.
6. Ma, L.; Liu, J. Catalytic Nucleic Acids: Biochemistry, Chemical Biology, Biosensors and Nanotechnology. *iScience* **2020**, *23*, 100815.
7. Wang, F.; Lu, C. H.; Willner, I. From Cascaded Catalytic Nucleic Acids to Enzyme-DNA Nanostructures: Controlling Reactivity, Sensing, Logic Operations, and Assembly of Complex Structures. *Chem. Rev.* **2014**, *114*, 2881–2941.
8. Travascio, P.; Bennet, A. J.; Wang, D. Y.; Sen, D. A Ribozyme and a Catalytic DNA with Peroxidase Activity: Active Sites Versus Cofactor-Binding Sites. *Chem. Biol.* **1999**, *6*, 779–787.
9. Travascio, P.; Li, Y. F.; Sen, D. DNA-Enhanced Peroxidase Activity of a DNA Aptamer–Hemin Complex. *Chem. Biol.* **1998**, *5*, 505–517.
10. Travascio, P.; Witting, P. K.; Mauk, A. G.; Sen, D. The Peroxidase Activity of a Hemin-DNA Oligonucleotide Complex: Free Radical Damage to Specific Guanine Bases of the DNA. *J. Am. Chem. Soc.* **2001**, *123*, 1337–1348.
11. Sen, D.; Poon, L. C. RNA and DNA Complexes with Hemin [Fe(III) Heme] Are Efficient Peroxidases and Peroxygenases: How Do They Do It and What Does It Mean? *Crit. Rev. Biochem. Mol. Biol.* **2011**, *46*, 478–492.
12. Roembke, B. T.; Nakayama, S.; Sintim, H. O. Nucleic Acid Detection Using G-Quadruplex Amplification Methodologies. *Methods* **2013**, *64*, 185–198.
13. Golub, E.; Albada, H. B.; Liao, W. C.; Biniuri, Y.; Willner, I. Nucleoapzymes: Hemin/G-Quadruplex DNAzyme-Aptamer Binding Site Conjugates with Superior Enzyme-Like Catalytic Functions. *J. Am. Chem. Soc.* **2016**, 138, 164–172.
14. Song, J.; Xu, C. H.; Huang, S. Z.; Lei, W.; Ruan, Y. F.; Lu, H. J.; Zhao, W.; Xu, J. J.; Chen, H. Y. Ultrasmall Nanopipette: Toward Continuous Monitoring of Redox Metabolism at Subcellular Level. *Angew. Chem. Int. Ed.* **2018**, *57*, 13226–13230.
15. Luo, G. F.; Biniuri, Y.; Vázquez-González, M.; Wulf, V.; Fadeev, M.; Lavi, R.; Willner, I. Metal Ion-Terpyridine-Functionalized l-Tyrosinamide Aptamers: Nucleoapzymes

for Oxygen Insertion into C–H Bonds and the Transformation of l-Tyrosinamide into Amidodopachrome. *Adv. Funct. Mater.* **2019**, *29*, 1901484.
16. Abe, H.; Abe, N.; Shibata, A.; Ito, K.; Tanaka, Y.; Ito, M.; Saneyoshi, H.; Shuto, S.; Ito, Y. Structure Formation and Catalytic Activity of DNA Dissolved in Organic Solvents. *Angew. Chem. Int. Ed.* **2012**, *51*, 6475–6479.
17. Hao, J.; Miao, W.; Cheng, Y.; Lu, S.; Jia, G.; Li, C. Enantioselective Olefin Cyclopropanation with G-Quadruplex DNA-Based Biocatalysts. *ACS Catal.* **2020**, *10*, 6561–6567.
18. Poon, L. C.; Methot, S. P.; Morabi-Pazooki, W.; Pio, F.; Bennet, A. J.; Sen, D. Guanine-Rich RNAs and DNAs that Bind Heme Robustly Catalyze Oxygen Transfer Reactions. *J. Am. Chem. Soc.* **2011**, *133*, 1877–1884.
19. Goertz, J. P.; White, I. M. Peroxidyme-Amplified Radical Chain Reaction (PARCR): Visible Detection of a Catalytic Reporter. *Angew. Chem. Int. Ed.* **2017**, *56*, 13411–13415.
20. Xing, Y.; Liu, X.; Pu, Q.; Wu, M.; Zhao, J. X. Biocompatible G-Quadruplex/Hemin for Enhancing Antibacterial Activity of $H_2O_2$. *ACS Appl. Bio. Mater.* **2018**, *1*, 1019–1027.
21. Einarson, O. J.; Sen, D. Self-Biotinylation of DNA G-Quadruplexes via Intrinsic Peroxidase Activity. *Nucleic Acids Res.* **2017**, *45*, 9813–9822.
22. Qi, C.; Zhang, N.; Yan, J.; Liu, X.; Bing, T.; Mei, H.; Shangguan, D. Activity Enhancement of G-Quadruplex/Hemin DNAzyme by Spermine. *RSC Adv.* **2014**, *4*, 1441–1448.
23. Stefan, L.; Denat, F.; Monchaud, D. Insights into How Nucleotide Supplements Enhance the Peroxidase-Mimicking DNAzyme Activity of the G-Quadruplex/Hemin System. *Nucleic Acids Res.* **2012**, *40*, 8759–8772.
24. Kong, D. M.; Xu, J.; Shen, H. X. Positive Effects of ATP on G-Quadruplex-Hemin DNAzyme-Mediated Reactions. *Anal. Chem.* **2010**, *82*, 6148–6153.
25. Stefan, L.; Duret, D.; Spinelli, N.; Defrancq, E.; Monchaud, D. Closer to Nature: An ATP-Driven Bioinspired Catalytic Oxidation Process. *Chem. Commun.* **2013**, *49*, 1500–1502.
26. Stefan, L.; Denat, F.; Monchaud, D. Deciphering the DNAzyme Activity of Multimeric Quadruplexes: Insights into Their Actual Role in the Telomerase Activity Evaluation Assay. *J. Am. Chem. Soc.* **2011**, *133*, 20405–20415.
27. Liu, Q.; Wang, H.; Shi, X.; Wang, Z. G.; Ding, B. Self-Assembled DNA/Peptide-Based Nanoparticle Exhibiting Synergistic Enzymatic Activity. *ACS Nano* **2017**, *11*, 7251–7258.
28. Wang, Z. G.; Li, Y.; Wang, H.; Wan, K.; Liu, Q.; Shi, X.; Ding, B. Enzyme Mimic Based on a Self-Assembled Chitosan/DNA Hybrid Exhibits Superior Activity and Tolerance. *Chem. Eur. J.* **2019**, *25*, 12576–12582.
29. Wang, Z.-G.; Wang, H.; Liu, Q.; Duan, F.; Shi, X.; Ding, B. Designed Self-Assembly of Peptides with G-Quadruplex/Hemin DNAzyme into Nanofibrils Possessing Enzyme-Mimicking Active Sites and Catalytic Functions. *ACS Catal.* **2018**, *8*, 7016–7024.
30. Wang, J.; Cheng, M.; Chen, J.; Ju, H.; Monchaud, D.; Mergny, J.-L.; Zhou, J. An Oxidatively Damaged G-Quadruplex/Hemin DNAzyme. *Chem. Commun.* **2020**, *56*, 1839–1842.
31. Li, W.; Li, Y.; Liu, Z.; Lin, B.; Yi, H.; Xu, F.; Nie, Z.; Yao, S. Insight into G-Quadruplex-Hemin DNAzyme/RNAzyme: Adjacent Adenine as the Intramolecular Species for Remarkable Enhancement of Enzymatic Activity. *Nucleic Acids Res.* **2016**, *44*, 7373–7384.
32. Nakayama, S.; Sintim, H. O. Colorimetric Split G-Quadruplex Probes for Nucleic Acid Sensing: Improving Reconstituted DNAzyme's Catalytic Efficiency via Probe Remodeling. *J. Am. Chem. Soc.* **2009**, *131*, 10320–10333.
33. Chen, J.; Guo, Y.; Zhou, J.; Ju, H. The Effect of Adenine Repeats on G-Quadruplex/Hemin Peroxidase Mimicking DNAzyme Activity. *Chem. Eur. J.* **2017**, *23*, 4210–4215.
34. Chen, J.; Zhang, Y.; Cheng, M.; Guo, Y.; Šponer, J.; Monchaud, D.; Mergny, J.-L.; Ju, H.; Zhou, J. How Proximal Nucleobases Regulate the Catalytic Activity of G-Quadruplex/Hemin DNAzymes. *ACS Catal.* **2018**, *8*, 11352–11361.
35. Chang, T.; Gong, H.; Ding, P.; Liu, X.; Li, W.; Bing, T.; Cao, Z.; Shangguan, D. Activity Enhancement of G-Quadruplex/Hemin DNAzyme by Flanking d(CCC). *Chem. Eur. J.* **2016**, *22*, 4015–4021.
36. Shinomiya, R.; Katahira, Y.; Araki, H.; Shibata, T.; Momotake, A.; Yanagisawa, S.; Ogura, T.; Suzuki, A.; Neya, S.; Yamamoto, Y. Characterization of Catalytic Activities and Heme Coordination Structures of Heme-DNA Complexes Composed of Some Chemically Modified Hemes and an All Parallel-Stranded Tetrameric G-Quadruplex DNA Formed from d(TTAGGG). *Biochemistry* **2018**, *57*, 5930–5937.
37. Liu, Y.; Lai, P.; Wang, J.; Xing, X.; Xu, L. A Superior G-Quadruplex DNAzyme Through Functionalized Modification of the Hemin Cofactor. *Chem. Commun.* **2020**, *56*, 2427–2430.
38. Zhu, L.; Li, C.; Zhu, Z.; Liu, D.; Zou, Y.; Wang, C.; Fu, H.; Yang, C. J. In Vitro Selection of Highly Efficient G-Quadruplex-Based DNAzymes. *Anal. Chem.* **2012**, *84*, 8383–8390.
39. Li, W.; Chen, S.; Xu, D.; Wen, Q.; Yang, T.; Liu, J. A DNA as a Substrate and an Enzyme: Direct Profiling of Methyltransferase Activity by Cytosine Methylation of a DNAzyme. *Chem. Eur. J.* **2018**, *24*, 14500–14505.
40. Yamamoto, Y.; Araki, H.; Shinomiya, R.; Hayasaka, K.; Nakayama, Y.; Ochi, K.; Shibata, T.; Momotake, A.; Ohyama, T.; Hagihara, M.; Hemmi, H. Structures and Catalytic Activities of Complexes Between Heme and All Parallel-Stranded Monomeric G-Quadruplex DNAs. *Biochemistry* **2018**, *57*, 5938–5948.
41. Sono, M.; Roach, M. P.; Coulter, E. D.; Dawson, J. H. Heme-Containing Oxygenases. *Chem. Rev.* **1996**, *96*, 2841–2888.
42. Berglund, G. I.; Carlsson, G. H.; Smith, A. T.; Szoke, H.; Henriksen, A.; Hajdu, J. The Catalytic Pathway of Horseradish Peroxidase at High Resolution. *Nature* **2002**, *417*, 463–468.
43. Vidossich, P.; Fiorin, G.; Alfonso-Prieto, M.; Derat, E.; Shaik, S.; Rovira, C. On the Role of Water in Peroxidase Catalysis: A Theoretical Investigation of HRP Compound I Formation. *J. Phys. Chem. B* **2010**, *114*, 5161–5169.
44. Poulos, T. L. Heme Enzyme Structure and Function. *Chem. Rev.* **2014**, *114*, 3919–3962.

DOI: 10.31635/ccschem.020.202000473
*CCS Chem.* **2020**, *2*, 2183–2193

45. Jones, P.; Dunford, H. B. The Mechanism of Compound I Formation Revisited. *J. Inorg. Biochem.* **2005**, *99*, 2292–2298.
46. Te Velde, G.; Bickelhaupt, F. M.; Baerends, E. J.; Fonseca Guerra, C.; Vangisbergen, S. J. A.; Snijders, J. G.; Ziegler, T. Chemistry with ADF. *J. Comput. Chem.* **2001**, *22*, 931–967.
47. Fonseca Guerra, C.; Snijders, J. G.; Te Velde, G.; Baerends, E. J. Towards an Order-N DFT Method. *Theor. Chem. Acc.* **1998**, *99*, 391–403.
48. Becke, A. D. Density-Functional Exchange-Energy Approximation with Correct Asymptotic Behavior. *Phys. Rev. A* **1988**, *38*, 3098–3100.
49. Lee, C.; Yang, W.; Parr, R. G. Development of the Colle-Salvetti Correlation-Energy Formula into a Functional of the Electron Density. *Phys. Rev. B* **1988**, *37*, 785–789.
50. Grimme, S.; Antony, J.; Ehrlich, S.; Krieg, H. A Consistent and Accurate Ab Initio Parametrization of Density Functional Dispersion Correction (DFT-D) for the 94 Elements H-Pu. *J. Chem. Phys.* **2010**, *132*, 154104.
51. Becke, A. D.; Johnson, E. R. A Density-Functional Model of the Dispersion Interaction. *J. Chem. Phys.* **2005**, *123*, 154101.
52. Cuervo, A.; Dans, P. D.; Carrascosa, J. L.; Orozco, M.; Gomila, G.; Fumagalli, L. Direct Measurement of the Dielectric Polarization Properties of DNA. *Proc. Natl. Acad. Sci. U. S. A.* **2014**, *111*, E3624–E3630.
53. Fonseca Guerra, C.; Handgraaf, J. W.; Baerends, E. J.; Bickelhaupt, F. M. Voronoi Deformation Density (VDD) Charges: Assessment of the Mulliken, Bader, Hirshfeld, Weinhold, and VDD Methods for Charge Analysis. *J. Comput. Chem.* **2004**, *25*, 189–210.
54. Rodriguez-Lopez, J. N.; Gilabert, M. A.; Tudela, J.; Thorneley, R. N.; Garcia-Canovas, F. Reactivity of Horseradish Peroxidase Compound II Toward Substrates: Kinetic Evidence for a Two-Step Mechanism. *Biochemistry* **2000**, *39*, 13201–13209.
55. Kamal, J. K. A.; Behere, D. V. Activity, Stability and Conformational Flexibility of Seed Coat Soybean Peroxidase. *J. Inorg. Biochem.* **2003**, *94*, 236–242.

DOI: 10.31635/ccschem.020.202000473
*CCS Chem.* **2020**, *2*, 2183–2193